


Connexin43 promotes angiogenesis through activating the HIF-1 α /VEGF signaling pathway under chronic cerebral hypoperfusion

Journal of Cerebral Blood Flow & Metabolism
2021, Vol. 41(10) 2656–2675
© The Author(s) 2021
Article reuse guidelines:
sagepub.com/journals-permissions
DOI: 10.1177/0271678X211010354
journals.sagepub.com/home/jcbfm


Weiwei Yu, Haiqiang Jin, Wei Sun, Ding Nan, Jianwen Deng, Jingjing Jia, Zemou Yu and Yining Huang 

Abstract

Chronic cerebral hypoperfusion, a major vascular contributor to vascular cognitive impairment and dementia, can exacerbate small vessel pathology. Connexin43, the most abundant gap junction protein in brain tissue, has been found to be critically involved in the pathological changes of vascular cognitive impairment and dementia caused by chronic cerebral hypoperfusion. However, the precise mechanisms underpinning its role are unclear. We established a mouse model via bilateral common carotid arteries stenosis on connexin43 heterozygous male mice and demonstrated that connexin43 improves brain blood flow recovery by mediating reparative angiogenesis under chronic cerebral hypoperfusion, which subsequently reduces the characteristic pathologies of vascular cognitive impairment and dementia including white matter lesions and irreversible neuronal injury. We additionally found that connexin43 mediates hypoxia inducible factor-1 α expression and then activates the PKA signaling pathway to regulate vascular endothelial growth factor-induced angiogenesis. All the above findings were replicated in bEnd.3 cells treated with 375 μ M CoCl₂ *in vitro*. These results suggest that connexin 43 could be instrumental in developing potential therapies for vascular cognitive impairment and dementia caused by chronic cerebral hypoperfusion.

Keywords

Chronic cerebral hypoperfusion, Connexin43, hypoxia inducible factor-1 α , angiogenesis, vascular cognitive impairment and dementia

Received 16 October 2020; Revised 14 March 2021; Accepted 18 March 2021

Introduction

Cerebrovascular disease (CVD) has been identified as the most common cause of vascular cognitive impairment and dementia (VCID).¹ While stroke has previously been considered as a cause of VCID, since the early 20th century impaired cerebral blood flow (CBF) regulation has been the dominant presumed mechanism underpinning VCID.^{2,3} Healthy CBF regulation involves a range of functions including enabling an adequate supply of oxygen and nutrients and maintaining the moment-to-moment adjustment of CBF to prevent hypoperfusion or hyperperfusion to the brain.⁴ If the CBF response to neuronal activation is impaired, the balance between the metabolic demand of the cerebral tissue and the supply of oxygen and nutrients may

be disrupted.⁵ Neurovascular uncoupling caused by even mild impairment of CBF regulation can adversely affect cerebral function.⁶ CBF regulation can be compromised in a range of types of blood vessels: cardiac,⁷ arterial, arteriolar or capillary.⁸ Chronic cerebral hypoperfusion (CCH), the most common consequence of CBF dysregulation, can lead to a protracted period of insufficient blood supply to the brain, which is a major vascular contributor to VCID⁹. There is growing

Department of Neurology, Peking University First Hospital, Beijing, China

Corresponding author:

Yining Huang, Department of Neurology, Peking University First Hospital, 8 Xishiku Street, Xicheng District, Beijing 100034, China.
Email: ynhuang@bjmu.edu.cn

evidence that maintaining cerebral perfusion via the dense microvascular network is critical for preserving normal cerebral function, including cognitive processing.^{9,10} Furthermore, low CBF can result in diffuse white matter (WM) damage, including the reduction of myelin and increase of axonal abnormalities.¹¹ WM changes are prevalent in nearly all subtypes of VCID,¹² suggesting that reduced perfusion to WM may play a critical role in VCID pathology. Additionally, CCH can exacerbate small vessel pathological lesions and the destruction of the blood brain barrier (BBB).¹³ These CCH-induced pathologies may be avoided by increasing the number of microvessels and consequently improving perfusion in the brain. Thus, an understanding of the factors affecting angiogenesis could provide vital opportunities to ameliorate brain damage at early stages.

Gap junctions (GJs) are specialized cell-to-cell channels formed by membrane proteins called connexins (Cx), which mediate cell communication by allowing the exchange of ions, second messengers and small molecules (<1.5 kDa) between cells.¹⁴ GJs provide efficient intercellular communication and gap junction intercellular communication (GJIC) is necessary to maintain homeostasis in organisms¹⁵ and essential for many physiological processes.^{16–18} Currently, there are known to be 21 Cxs expressed in the human genome,^{19,20} 11 of which can be detected in the brain.^{21,22} Connexin 43 (Cx43) is the most abundant connexin in the brain and has been reported to be involved in many pathophysiological central nervous system (CNS) states,²³ such as stroke,²⁴ Alzheimer's disease (AD),²⁵ Parkinson's disease (PD)²⁶ and epilepsy.²⁷ Relevant to the current study, Cx43 has been found to be involved in angiogenesis.²⁸ For example, a previous study found that angiotensin II enhanced angiogenesis by increasing the formation of Cx43 GJs, improving the outcome of mesenchymal-stem-cells-based (MSCs) therapy for myocardial infarction (MI).²⁹ Cx43-stimulated angiogenesis is also found in wound healing promoted by bioglass.³⁰ Interestingly, Cx43 deficiency in astrocytes can attenuate the pathological changes of VCID, which is characterized by demyelination and cognitive decline associated with CCH.³¹ However, the effect of Cx43 deletion in endothelial cells (ECs) on cerebrovascular angiogenesis in CCH-induced VCID is less well understood.

Hypoxia inducible factor-1 (HIF-1) is comprised of two basic proteins: HIF-1 α , which is regulated by both O₂ and the other HIF-1 component protein, HIF-1 β .³² HIF-1 has been identified as an essential regulator for gene expression especially in hypoxic conditioning.³³ HIF-1 α is constitutively expressed in various cell types and its half-life is less than 5 min due to being constitutively degraded by prolyl-hydroxylase enzymes

under normoxic conditions.³⁴ However, hypoxia inhibits the prolyl-hydroxylase enzymes which stabilize HIF-1 α . Previous studies have found that HIF-1 α promotes angiogenesis induced by vascular endothelial growth factor (VEGF).^{35,36} However, it is unclear whether the expression of HIF-1 α and VEGF during angiogenesis can be mediated by Cx43 under hypoxic conditions. In order to examine this possibility, we used Cx43 genetically engineered mice to explore whether Cx43 deficiency affects early stages of CCH-induced VCID by mediating cerebrovascular angiogenesis and whether the underlying mechanism involves the HIF-1 α /VEGF pathway.

Materials and methods

Animals

C57BL/6J mice that were globally heterozygous for Cx43 (Cx43^{+/-}) as a result of employing CRISPR/Cas-9 gene-targeting technology were obtained from Shanghai Biomodel Organism Science & Technology Co (China). Cx43^{+/-} mice were bred in the specific pathogen-free (SPF) animal facility of the Peking University First Hospital. Genotyping of the breeding mice was performed using PCR technology. The primer sequences were as follows: primer 1 (5'-GCTGAA GGTCCGTCCTCAA-3'); primer 2 (5'-TCCACA CCTAGAAAATCAGG-3'); primer 3 (5'-GCAGAC TGTTTCATCACCCCA-3'). All mice were housed with a 12-h light/dark cycle and had free access to food and water. All experiments on mice were performed with the approval of the Ethics Committee of Peking University First Hospital. Animal experiments were conducted in compliance with the National Institutes of Health Guide for the Care and Use of Laboratory Animals and the ARRIVE 2.0 guidelines were followed for reporting animal experiments.³⁷

Mouse model of CCH

The CCH mouse model was established using bilateral common carotid arteries stenosis (BCAS). Twelve-week-old male mice were randomly assigned to four experimental groups: Cx43^{+/+} +sham, Cx43^{+/-} +sham, Cx43^{+/+} +BCAS, Cx43^{+/-} +BCAS. We performed BCAS using microcoils with an inner diameter of 0.18 mm (Sawane Spring, Japan), as previously described.³⁸ Briefly, mice were anesthetized with 1% sodium pentobarbital and common carotid arteries (CCAs) were isolated from their sheaths under stereomicroscope. The microcoils were gently twined around both CCAs just proximal to the carotid bifurcation, 30 min apart. Sham-operated mice had the same surgery performed, except for twining the microcoils.

Thirty days after BCAS, mice were prepared for the experimental studies described below.

CBF measurement

CBF was measured by a Laser Doppler perfusion image system (Peri Scan PIM3 System; PERIMED, Stockholm, Sweden) as described in previous publications.^{39,40} An incision was made through the scalp of the anesthetized mice and the skull was fully exposed by retracting the skin as well as removing the connective tissue adhered to the skull using a sterile cotton swab. An optical scanner controlled by the computer directed a low-powered He-Ne laser beam over the whole exposed skull. The exposure procedure took 20 milliseconds with 25 frames. A color-coded image indicating relative perfusion levels was shown on a video monitor⁴¹ and all images obtained before the BCAS (baseline), 5 min after the BCAS and 30 days after the BCAS were analyzed with the LDPIwin 3.1 software (PeriScan PIM3 System; PERIMED, Stockholm, Sweden).

Hypoxia studies with pimonidazole in vivo

The HypoxyprobeTM-1(HP-1, Burlington, MA, USA, HP1-100Kit) immunofluorescent analysis can be used to evaluate the hypoxia in brain tissues with a pO₂ below 10 mmHg, as previously described.⁴² Briefly, the HypoxyprobeTM (pimonidazole) is resuspended at a concentration of 30 mg/ml in 0.9% sterile saline. The mice were injected with the pimonidazole solution at a recommended dose of 60 mg/kg through the tail veins after the surgery. After 90 minutes of pimonidazole circulation *in vivo*, the mice were anesthetized intraperitoneally with 40 mg/kg sodium pentobarbital and transcardially perfused with PBS. Subsequently, brains were typically harvested and placed in a cryo-embedding medium (Sakura-Finetek USA 4583). The embedded brains were cut into 7- μ m thick sections that were placed on microscope slides for staining. After being fixed in cold acetone for 10 min, the sections were washed with PBS three times and blocked with 10% normal goat serum for 1 h at RT. Subsequently, the sections were incubated overnight at 4°C with mouse monoclonal anti-pimonidazole antibody (MAb1) at a 1/50 dilution in PBS. After being washed with PBS three times, the slides were then incubated with secondary antibody conjugated with FITC (ZSGB-Bio, ZF-0311, 1:100) for 1 h at RT. Finally, the slides ultimately were mounted with mounting solution DAPI (ZSGB-Bio, ZLI-9557) and a coverslip. Fluorescence images were captured using a fluorescence microscope (Ti2E, Nikon, Tokyo, Japan). The mean fluorescence intensity (MFI) of the fluorescence staining was quantified using the ImageJ software.

Immunohistochemistry

Thirty days after surgery, mice were anesthetized intraperitoneally with 40 mg/kg sodium pentobarbital and transcardially perfused with phosphate buffer saline (PBS). Brains were dissected, post-fixed in 4% paraformaldehyde (PFA) for 24 h and equilibrated in a 30% sucrose solution. Brain tissues were embedded in paraffin and sectioned at 4 μ m. The paraffin-embedded brain sections were used for IHC studies. The brain sections were deparaffinized, rehydrated, subjected to antigen retrieval (EDTA PH=9 ZLI-9086) and incubated with 10% normal goat serum (ZSGB-Bio, ZLI-9021). Subsequently, sections were incubated overnight at 4°C with the primary antibody, anti-CD31 polyclonal antibody (Abcam, ab28364, 1:100). The next day, the brain sections were incubated with secondary antibodies for one hour at room temperature (RT) and treated with diaminobenzidine (DAB). The sections were observed by light microscopy. The capillary density was analyzed using Image Pro-Plus software (Media Cybernetics, Inc, Rockville, MD). The capillary length was measured using the Image J plug-in "Neuro J" length analysis tool.

Multiphoton in vivo microscopy analysis

30 days after surgery, cranial windows were prepared as previously described.⁴³ In brief, mice were anesthetized intraperitoneally with 1% sodium pentobarbital and the head was secured in a stereotactic frame. A 1.0 cm incision was made in the middle of the scalp and a square parietal window was created with a hand-held drill. The dura was eliminated and the exposed brain was covered continuously with 37°C warm PBS. Only mice without any bleeding from the cranial window were included in the study. Fluorescein-conjugated mega-dextran (2,000,000 Da, 0.1 ml of 10 mg/ml, Invitrogen, D7137) was injected via the tail vein to investigate the perfused capillary, while Fluorescein-conjugated mega-dextran (40,000 Da, 0.1 mL of 10 mg/ml, Invitrogen, D1844) was used to observe the permeability of the BBB at 5, 15 and 30 min after the injection. Z-stack *in vivo* images were immediately acquired through the cranial window by a two-photon microscope (Nikon, Tokyo, Japan) with 488 nm excitation. The length of cortical microvascular (≤ 6 μ m in diameter) was determined using the Image J plug-in "Neuro J" line segment analysis tool as previously described.⁴⁴

Hematoxylin-eosin staining

The paraffin-embedded slides obtained 30 days after surgery were first deparaffinized by xylene treatment three times for 10 min followed by rehydrating

gradually through different alcohol grades from 100 to 70%. Subsequently, sections were stained with hematoxylin for 1 min and the remaining stain was washed with PBS. Sections were then treated with eosin stain for 30 s and dehydrated by passing through 70 to 100% ethanol and xylene transparent. Finally, sections were covered by a cover slip and observed with a light microscope to study the WM in corpus callosum (CC) and hippocampal neurons.

Tissue immunofluorescence and confocal microscopy

Paraffin-embedded brain sections as described above were also used for IF analyses. The sections were treated the same as in the IHC analyses until the step of being blocked with 10% normal goat serum. Subsequently, the sections were individually incubated with the following antibodies: anti-glia fibrillary acidic protein polyclonal antibody (GFAP, Abcam, ab7260, 1:100), anti-myelin-basic-protein polyclonal antibody (MBP, Proteintech, 10458-1-AP, 1:100) and anti-myelin-associated glycoprotein polyclonal antibody (MAG, Proteintech, 14386-1-AP, 1:100). Additionally, Ki-67 (Cell Signaling Technology, 9129 T, 1:100) and CD31 (Abcam, ab24590, 1:200) double-staining were performed. After an overnight incubation at 4°C, the sections were washed in PBS and applied with secondary antibodies conjugated with FITC (ZSGB-Bio, ZF-0311, 1:100) for 1 h at RT. Finally, the sections were covered with slips using fluorescent mounting medium containing DAPI (ZSGB-Bio, ZLI-9557). Fluorescence images were observed using a fluorescence microscope (Ti2E, Nikon, Tokyo, Japan).

Prolonged hypoxic conditions in vitro

Immortalized mouse brain microvascular endothelial cells from the cell line bEnd.3 derived from mice were purchased from the American Type Culture Collection (ATCC; Manassas, VA, USA). Cells were grown in DMEM (Thermo Fisher Scientific) supplemented with 10% fetal bovine serum (FBS, Thermo Fisher Scientific) and 100 U/ml penicillin and streptomycin (Thermo Fisher Scientific) and maintained in a humidified incubator (95% air/5% CO₂; Thermo Fisher Scientific, Waltham, MA, USA) at 37°C. Cells were treated with Cobalt chloride (CoCl₂, 0, 62.5, 125, 250, 375, 500 μM, sigma, C8661) for 24 h when growing to 80% confluence in order to induce prolonged hypoxic conditions.⁴⁵ In order to identify the optimal concentration of CoCl₂ solution, we measured HIF-1α expression and employed Cell Counting Kit 8 (CCK-8) reagent (1:10 dilution in medium; Dojindo, Kumamoto, Japan).

Transfection and CoCl₂ treatment

Cells were cultured in 6-well plates to 70% confluence and transiently transfected with 2.5 μg of plasmid with LipofetamineTM 2000 Reagent (Invitrogen, Carlsbad, CA, USA) according to the manufacturer. For Cx43 siRNA, cells were transfected with 20 μM of siRNA against Cx43 (siCx43 sense: 5'-CCCAACUGAAC CUUAAGAATT-3', antisense: 5'-UUCUUAAGG UUCAGUUGGGTT-3'),⁴⁶ and negative control siRNA (NC-siRNA, sense: 5'-UUCUCCGAACGUG UCACGUTT-3', antisense: 5'-ACGUGACACGUUC GGAGAATT-3') was used as a control. The transfected cells were incubated at 37°C with 5% CO₂ for 72 h, but the culture medium was replaced with fresh DMEM containing 10% FBS to remove the calcium-phosphate precipitate 24 h post-transfection. Additionally, the cells were treated with 375 μM CoCl₂ in the last 24 h of siRNA transfection. After the treatment, the cells were prepared for the ELISA assay described below.

ELISA assay for VEGF

The concentration of VEGF in the culture medium of each group was assessed using an VEGF ELISA kit (RayBiotech, Atlanta, United States, ELM-VEGF). Aliquots of 100 μl standard or sample were added to the appropriate microplate wells provided by the ELISA kit and then incubated for 2.5 h at RT. After discarding the liquid from each well, 100 μl of prepared biotinylated anti-mouse VEGF antibody was added to each well and incubated for 1 h at RT. After washing three times, 100 μl of prepared Streptavidin solution was added to each well and incubated for 45 min at RT with gentle shaking. Finally, 100 μl TMB One-Step Substrate Reagent was added and incubated for 30 min at RT in the dark before 50 μl of stop solution was added to each well. The absorbance was measured at 450 nm on a microplate reader. The concentrations of unknown samples were obtained from the generated standard curve.

Scratch migration assay

The migration ability of bEnd.3 cells was assessed by a scratch assay. Cells in four groups (NC-siRNA, Cx43-siRNA, NC-siRNA+CoCl₂, Cx43-siRNA+CoCl₂), treated as described in the previous section, were cultured until they reached 90% confluence in 3.5 cm culture dishes. Confluent cell monolayers were scratched in a straight line using a 1250 μl pipet tip to form wounded gaps. The culture medium containing debris was discarded and the cells were washed with PBS three times to smooth the edge of the scratch. The cells were then cultured with serum-free DMEM medium in the

incubator (37°C and 5% CO₂) for 24 h. The wounded gaps were photographed from three different areas for each wound on a microscope at 0 h and 24 h later. To capture the same field during image collection, we made some marks as reference signs close to the scratch. Finally, the degree of cell migration was calculated using ImageJ software v.1.37 (National Institutes of Health, Bethesda, MD, USA). Quantifications of migratory areas were expressed as a percentage of decreased area to the initial area at 0 h.

Cellular IF and confocal microscopy

Cells were fixed with freshly made -20°C Ethanol or 4% paraformaldehyde. After being treated with 0.2% Triton X-100 in PBS, cells were blocked with 10% goat serum at RT for 1 h. Cells were then incubated with primary antibodies against zonula occludens-1 (ZO-1; 1:50; Proteintech; 21773-1-AP) and claudin-5 (1:100; Abcam; ab15106) at 4°C overnight. Corresponding TRITC-conjugated secondary antibodies (1:100; ZSGB-Bio) were then applied to cells for 1 h at RT in the dark. Cells were mounted with mounting medium containing DAPI (ZSGB-Bio) and fluorescence images were obtained by a fluorescence microscope (Ti2E, Nikon, Tokyo, Japan).

Western blotting analysis

Isolated brains from mice 30 days after surgery or cultured cells were lysed in SDS Lysis Buffer (P0013G, Beyotime, China) containing 1 mM Phenylmethanesulfonyl fluoride (PMSF, ST506, Beyotime, China). Protein concentration of the samples was determined using a Pierce BCA Protein Assay kit (Thermo Scientific™, USA). Equal volumes of extract protein (30 µg) were subjected to 10% SDS/PAGE gel electrophoresis and transferred to PVDF membranes (MilliporeSigma), which were then blocked with 5% non-fat milk powder in Tris-buffered saline containing 0.1% Tween-20 (TBST) for 60 min at RT. Subsequently, membranes were incubated with the following primary antibodies overnight at 4°C: Anti-claudin-5 (1:1000, Abcam, ab15106), Anti-ZO-1 (1:1000, Proteintech, 21773-1-AP), Anti-Cx43 (1:1000, Cell Signaling Technology, 3512S), Anti-Akt (1:1000, Cell Signaling Technology, 4685S), Anti-phospho-Akt (Ser473) (1:1000, Cell Signaling Technology, 4060S), Anti-HIF-1α (1:1000, Abcam, ab179483), Anti-GFAP (1:1000, Abcam, ab7260), Anti-MBP (1:1000, Proteintech, 10458-1-AP), Anti-MAG (1:1000, Proteintech, 14386-1-AP), Anti-β-actin (1:1000, ZSGB-Bio, TA-09), and Anti-GAPDH (1:1000, ZSGB-Bio, TA-09). Antigen-antibody complexes were incubated with goat anti-mouse or rabbit

horseradish peroxidase (HRP)-conjugated secondary antibodies (1:6000, ZSGB-Bio, ZB-2301, ZB-2305) for 1 h at RT. Protein bands were visualized using ECL (Millipore Sigma) with a detection system (GBOX-CHEMI-XT4, GENE, Hong Kong, China). Optical densities of each band were measured using ImageJ software v.1.37 (National Institutes of Health, Bethesda, MD, USA) and results were normalized to GAPDH in each sample lane.

Real time-polymerase chain reaction

Total brain RNA was extracted from mice 30 days post-surgery using Trizol reagent (Thermo Fisher Scientific) and was reverse transcribed by reverse transcriptase according to the manufacturer's instructions (TransGen Biotech, AT301-03) in order to produce cDNA. The cDNA was added to a 20 µl reaction volume including SybrGreen Master Mix (Thermo Fisher Scientific) and PCR primers. RT-PCR was performed by a 7500 Real-Time PCR System (Thermo Fisher Scientific). The sequences were as follows: HIF-1α: (F) 5'-ACCTTCATCGGAAACTCCAAAG-3', (R) 5'-CTGTTAGGCTGGGAAAAGTTAGG-3'; VEGF: (F) 5'-AGAAAGCCCATGAAGTGGTG-3', (R) 5'-ACTCCAGGGCTTCATCATTG-3'; β-actin: (F) 5'-ACTATCGGCAATGAGCGGTTCC-3', (R) 5'-AGCACTGTGTTGGCATAGAGGTC-3'. Relative fold changes were calculated by the 2^{-ΔΔC_t} method.

Statistical analysis

Statistical analysis was performed using GraphPad Prism 7.0 software (GraphPad Software, Inc., La Jolla, CA, USA), and the Kolmogoroc-Smirnov D test (K-S test) was used to test for normality. Results are summarized and displayed as mean ± standard deviation (SD). Significant group differences were examined for multiple group comparisons using one-way ANOVA followed by Bonferroni post hoc tests, and for two group comparisons using Student's t-tests. If data was non-normally distributed, a non-parametric test was used to assess group differences. A value of P < 0.05 was taken as the threshold for significance.

Results

Cx43 mediates brain blood flow recovery after the CCH

Because Cx43 homozygous knock-out mice die neonatally of pulmonary outflow tract obstruction,⁴⁷ we generated Cx43 heterozygous mice to study the role of Cx43 in angiogenesis. PCR analysis of Cx43

heterozygous mice indicated a 4.2 kb wild band and 2.5 kb mutant band (Figure 1(a)). Immunoblot analysis revealed that Cx43 protein expression in Cx43^{+/-} mice was reduced by approximately 50% compared with Cx43^{+/+} mice (Figure 1(b) and (c)). The results of PCR and immunoblot prove that Cx43 gene has been successfully knocked down in the brain tissue. Simultaneously, we performed magnetic resonance angiography (MRA) experiment to ensure if genetic knockdown of Cx43 can affect the development of cerebral vasculature. The results of MRA demonstrate no difference in cerebral vasculature between Cx43^{+/+} and Cx43^{+/-} mice, whether viewed from the bottom (left) or sagittal (right) side of the brains (Figure S1 (a)), which suggests that Cx43 knockdown has no effect on the development of cerebral vasculature. Figure 1(d) shows the CCA pre- and post-BCAS surgery, and the narrowing of the CCA following surgery is evident. To verify whether the surgery was successful, we measured the CBF before and after the BCAS surgery using Laser Doppler. The results showed that the CBF of BCAS groups was decreased to approximately 20% (Cx43^{+/+}: 18.83 ± 1.06%, Cx43^{+/-}: 18.12 ± 1.101%) of the CBF in the sham-operated groups; there were no differences in CBF between Cx43^{+/+} and Cx43^{+/-} mice in the sham- or BCAS-operated groups (Figure 1(e) and (f)). Additionally, a hypoxyprobe kit was used to assess the hypoxia in the brains as described in the Materials and Methods section. The results revealed a significantly stronger hypoxic signal in the BCAS-operated group compared to the sham-operated group (Figure 1(g)). The quantification of mean fluorescence intensity (MFI) showed no statistical difference between the BCAS-operated Cx43^{+/+} group and the Cx43^{+/-} mice groups (Figure 1(h)). Thirty days after BCAS, the CBF in the BCAS-operated Cx43^{+/+} mice demonstrated a moderate recovery (71.43 ± 2.588%) whereas Cx43^{+/-} mice had poor recovery (40.55 ± 5.101%) (Figure 1(i) to (j)). These results suggest that Cx43 is necessary for collateral vessel establishment in response to hypoxia induced by CCH.

Cx43 mediates CCH-induced reparative angiogenesis after BCAS

One of the advantages of a BCAS mouse model is that it can offer a unique platform for investigating the mechanisms of angiogenesis and contribute to the study of potential drugs to enhance angiogenesis.⁴⁸ We performed IHC analysis staining with CD31, in order to observe capillary density. The results clearly indicate new capillary formation in both the cortex and striatum of BCAS-operated Cx43^{+/+} mice, but not in those of BCAS-operated Cx43^{+/-} mice (Figure 2(a)).

Quantification of capillaries stained with CD31 in the cortex and striatum indicated that capillary density was approximately 2 (cortex) and 1.5 (striatum) fold lower in BCAS-operated Cx43^{+/-} mice than that in Cx43^{+/+} mice and capillary length in BCAS-operated Cx43^{+/-} mice was significantly longer than that in Cx43^{+/+} mice (Figure 2(b)). There was no significant difference in capillary density between sham-operated Cx43^{+/+} and Cx43^{+/-} mice (Figure 2(a) and (b)). To further evaluate whether Cx43 mediates the CCH-induced angiogenesis after BCAS, we performed the Ki-67 and CD31 IF double-staining. The results showed the number of cortical Ki-67/CD31 double-positive cells was significantly lower in the BCAS-operated Cx43^{+/-} mice compared to Cx43^{+/+} mice (Figure 2(c)). VEGF, which plays a critical role in angiogenesis, was evaluated by immunoblot analysis. 7 days after BCAS surgery, an obvious increase of VEGF expression was observed in the whole brain of BCAS-operated Cx43^{+/+} mice, but not in those of BCAS-operated Cx43^{+/-} mice (Figure S2(a)). The quantitative analysis revealed an approximate 1.5 fold of VEGF expression in BCAS-operated Cx43^{+/+} mice compared to Cx43^{+/-} mice (Figure S2 (b)). Notably, the increased VEGF expression in BCAS-operated Cx43^{+/+} mice lasted until 30 days after surgery (Figure 2(d)), although it was near 1.3 fold compared with BCAS-operated Cx43^{+/-} mice (Figure 2(e)). There was no difference between sham-operated Cx43^{+/-} mice and Cx43^{+/+} mice (Figure 2(d) and (e)). These findings indicate that there is a significant relationship between Cx43 deficiency and impaired capillary density during CCH.

In order to further examine *in vivo* how microvascular reductions reflect capillary perfusion deficits, we obtained angiograms using multiphoton microscopy imaging with 2,000,000 Da FITC-conjugated dextran. Deficits in functional microvasculature formation were visualized by blood perfusion of FITC-conjugated dextran. The angiograms of the four groups indicated that the BCAS-operated Cx43^{+/-} mice exhibited significantly reduced microvascular perfusion compared to BCAS-operated Cx43^{+/-} mice (Figure 2(f)). The quantitative analysis of these angiograms has demonstrated a significant 46% reduction of perfused capillary length in BCAS-operated Cx43^{+/-} mice compared to BCAS-operated Cx43^{+/+} mice (Figure 2(g)), which is comparable to the reductions determined by histological analysis. The above results indicated that Cx43 deficiency impairs VEGF-induced angiogenesis.

Cx43 deficiency disrupts BBB integrity

Previous studies have found that barrierogenesis occurs simultaneously with brain angiogenesis and that the special barrier features of BBB ECs are induced

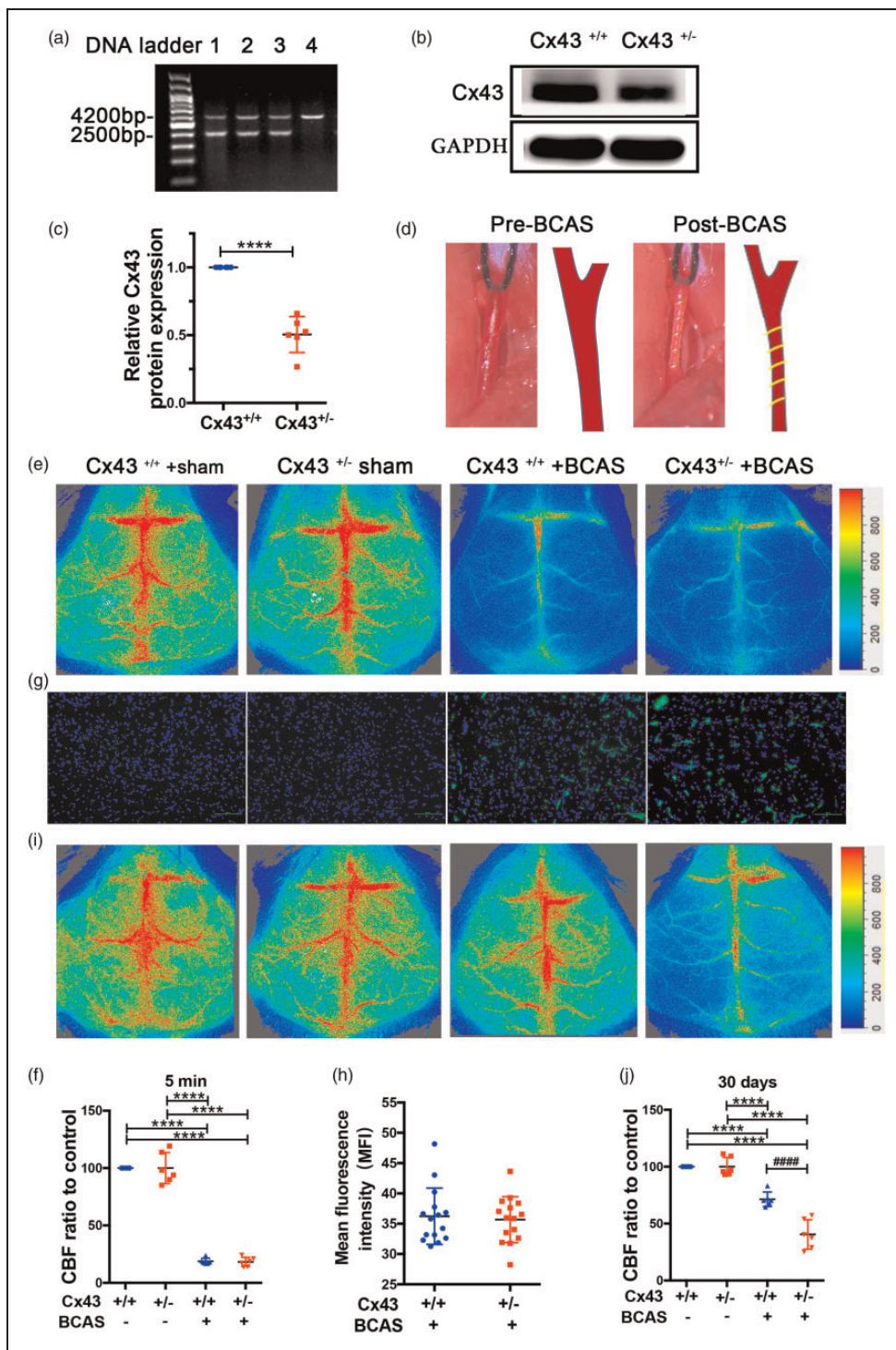


Figure 1. Cx43 KO mice manifested flawed brain blood flow recovery in response to CCH. PCR (a) and immunoblot (b) were performed to evaluate the genotype of Cx43 KO mice. (a) Genomic DNA from Cx43 WT and KO mice were subjected to PCR using the primers for genotyping. (b) Brains isolated from Cx43 WT and KO mice were lysed and the expression levels of Cx43 were examined using GAPDH as a loading control. (c) Analysis of optical densities of the bands. **** $P < 0.0001$, $n = 6$ mice for each group. (d) Representative photographs of CCA before (left) and after (right) placement of a microcoil. (e) Laser Doppler was used to monitor CBF before and 5 min after BCAS surgery. (f) Quantitative analysis of CBF using percentage of the ischemic brain relative to the control brain. (g) Representative images of pimonidazole adducts in the cerebral tissue of the four mouse groups. Scale bar = 100 μm . (h) The average fluorescence intensity of the hypoxic area was analyzed in the brains of the BCAS-operated group mice using a Student's t -test. (i) 30 days after the surgery, Laser Doppler was used to analyze CBF in the four mouse groups. (j) A quantitative comparison of CBF in Figure 1(i) using percentage relative to the sham-operated mice. **** $P < 0.0001$ versus sham-operated mice, #### $P < 0.0001$ versus BCAS-operated Cx43^{+/+} mice, $n = 6$ mice in each group.

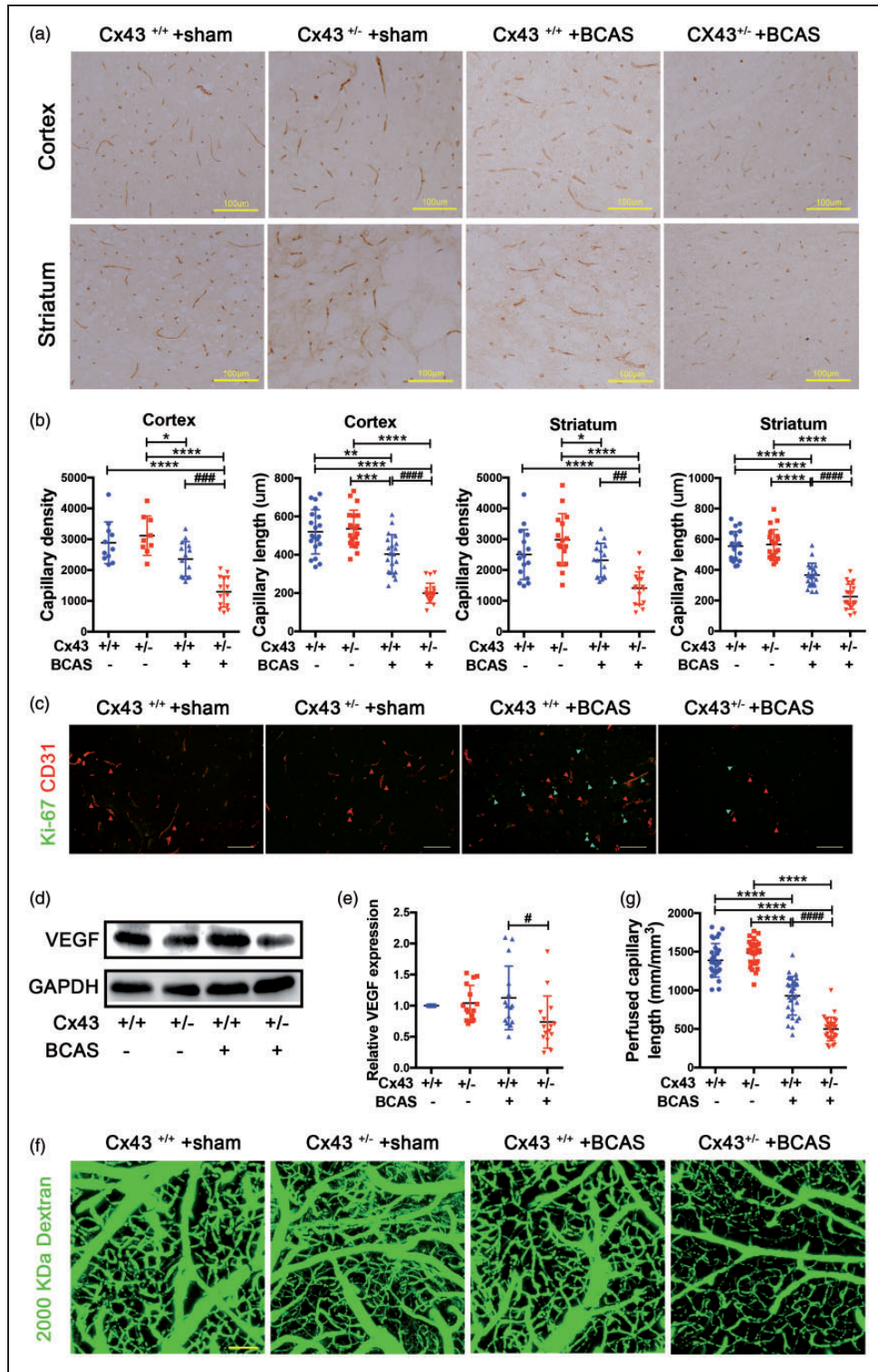


Figure 2. Cx43 KO mice displayed defective reparative angiogenesis after BCAS. (a) Immunohistochemical analysis of CD31 in the cortex and striatum of the brain slices removed from the four mouse groups 30 days after surgery. Brown strips indicated CD31-positive capillaries. Scale bar = 100 μ m. (b) Quantification of density and length of CD31-positive capillaries in the cortex and striatum. (c) Ki-67 and CD31 immunohistochemical double-staining. Ki-67 was stained in green and CD31 in red. Scale bar = 100 μ m. (d) Immunoblot analysis of VEGF expression of brain tissues with GAPDH used as loading control. (e) Quantitative analysis of VEGF relative to GAPDH. (f) Cortical microvascular perfusion was evaluated by *in vivo* multiphoton microscopy analysis of 2,000,000 Da FITC-conjugated dextran. Scale bar = 100 μ m. (g) Quantitative analysis of perfused capillary length from angiograms in Figure 2(f). ***P < 0.0001 **P < 0.001 *P < 0.01 #P < 0.05 versus sham-operated mice, #####P < 0.0001 ####P < 0.001 ###P < 0.01 #P < 0.05 versus BCAS-operated Cx43^{+/+} mice, n \geq 6 mice in each group.

during brain angiogenesis.^{49,50} Additionally, previous reports suggest that murine CCH can result in the disruption of BBB integrity, and this is a precursor to significant white matter lesions (WMLs) or cognitive deficits.⁵¹ However, it is unknown whether impaired angiogenesis in Cx43-deficient mice can influence BBB permeability during CCH. To test for this possibility, we observed the cortical vessels *in vivo* using time-lapse multiphoton imaging with intravenous 40,000 Da FITC-conjugated dextran. In contrast to BCAS-operated Cx43^{+/+} mice who had intact BBB in response to 40,000 Da FITC-conjugated dextran, throughout the 30 min of imaging, there was leakage of FITC-conjugated dextran in Cx43^{+/-} mice at 15 min (white arrow) which progressively increased until 30 min (white arrow) (Figure 3(a)). There was an approximate 2 fold leakage of FITC-conjugated dextran in Cx43^{+/-} mice compared to Cx43^{+/+} mice at 30 min (Figure 3(b)). To further evaluate our *in vivo* multiphoton results, we performed western blotting for the tight junction proteins to analyze the integrity of the BBB. The results were consistent with the imaging *in vivo*: after BCAS, the expression of ZO-1 (P=0.048) and claudin-5 (P=0.017) decreased in Cx43^{+/-} mice compared to Cx43^{+/+} mice (Figure 3(c) and (d)). There was no difference between sham-operated Cx43^{+/-} mice and Cx43^{+/+} mice. Together, with the impaired angiogenesis under CCH in Cx43 deficient mice, BBB integrity is simultaneously disrupted.

Endothelial dysfunction is involved in the pathogenesis of VCID after CCH

WMLs and neuronal injury, which are key features of VCID, can be experimentally induced by CCH.⁵² In the next set of analysis we aimed to discern whether Cx43 deficiency, which impairs microvascular function and BBB integrity, would be sufficient to induce the pathogenesis of VCID after BCAS. HE staining was used to evaluate the histological changes to the CC and hippocampus. The results indicated no difference in WM integrity between sham-operated Cx43^{+/+} mice and Cx43^{+/-} mice. The two groups of BCAS-operated mice had pathological changes, including disarrangement of the nerve fibers and reduction of myelinated fibers (Figure 4(a), indicated in the area between the two yellow dotted lines). Within the BCAS-operated groups, the WM of Cx43^{+/-} mice was more vulnerable to injury than that of Cx43^{+/+} mice (Figure 4(a)). The results of hippocampus HE staining indicated a moderate loss of neurons in CA1 stratum pyramidal for BCAS-operated Cx43^{+/-} mice compared to Cx43^{+/+} mice (Figure 4(e), indicated by the white arrows). Hippocampal neuron counts were significantly lower

in BCAS-operated Cx43^{+/-} mice compared to the other three groups (Figure 4(f)). Simultaneously, we performed Morris water maze to evaluate the spatial learning and memory ability of mice. The results revealed that the escape latency of sham-operated mice decreased progressively through the training while BCAS-operated mice showed a poorer spatial learning ability from day 2 to day 5, especially BCAS-operated Cx43^{+/-} mice (Figure 4(g), P<0.0001 versus sham-operated mice and P<0.01 versus BCAS-operated Cx43^{+/+} mice on the 5th day).

WM integrity was subsequently assessed with IF staining and western blot, including GFAP, MBP and MAG. As expected, BCAS-operated mice showed a degradation of WM integrity in the CC. GFAP-stained astrocytes were more activated in BCAS-operated Cx43^{+/-} mice compared with Cx43^{+/+} mice, as evidenced by shorter and wider processes and enhanced GFAP staining (Figure 4(b)). Additionally, the attenuation of myelinated fibers and the reduction of MBP and MAG in BCAS-operated mice were both more severe in Cx43^{+/-} mice compared with Cx43^{+/+} mice (Figure 4(b)). Western blot analyses revealed that the expression of MBP (P=0.0168) and MAG (P=0.0021) significantly decreased in BCAS-operated Cx43^{+/-} mice compared to BCAS-operated Cx43^{+/+} mice (Figure 4(c) and (d)), while there was no difference in GFAP expression between BCAS-operated Cx43^{+/-} and Cx43^{+/+} mice (Figure 4(c) and (d)). These results suggest that angiogenesis attenuates WML pathogenesis and irreversible neuronal injury after BCAS.

Cx43 may mediate HIF-1 α expression to activate the PKA signaling pathway, which is required for VEGF-induced angiogenesis

We next examined whether under CCH the HIF-1 α pathway is involved in the process of Cx43 mediating VEGF-induced reparative angiogenesis. Similarly, we assessed HIF-1 α expression using western blotting 7 days after the surgery. HIF-1 α expression was low in both sham-operated groups but was significantly elevated in BCAS-operated group mice, especially in Cx43^{+/+} mice compared to Cx43^{+/-} mice (2.6 fold) (Figure S2(a) and (b)). Previous studies have found that HIF-1 α expression is primarily regulated by the protein kinase B (AKT) signaling pathway⁵³ and this signaling pathway is involved in the proliferation, differentiation and survival of a variety of cell types.⁵⁴ In order to characterize the role of AKT in the Cx43 regulation of the HIF-1 α /VEGF signaling pathway, we assessed the expression of AKT and p-AKT. We found that AKT total expression level did not differ between the groups (Figure S2(a) and (b)). However,

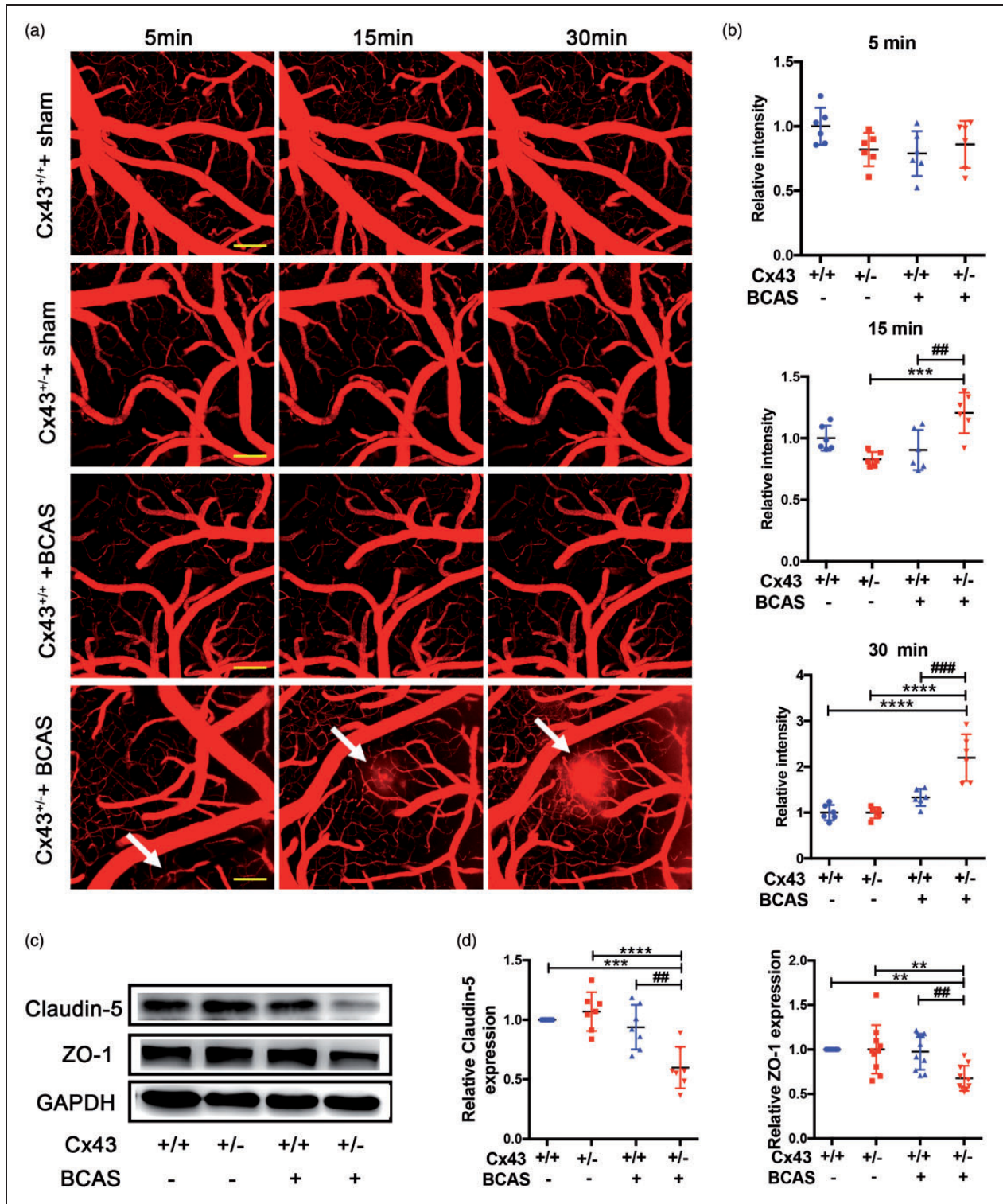


Figure 3. BBB disruption in Cx43-deficient mice under CCH. (a) 30 days after BCAS, *in vivo* multiphoton imaging of 40,000 Da FITC-conjugated dextran leakage from microvasculature at 5 min, 15 min, and 30 min after FITC-dextran intravenous administration. Scale bar = 100 μm. (b) Quantitative analysis of the relative fluorescence intensity across a cross-section of vessels from each group in Figure 3 (a) using NIH image J software. (c) Western blots showing the integrity of the BBB under CCH by analyzing the levels of claudin-5 and ZO-1. (d) Quantitative analysis of protein levels relative to GAPDH. ****P < 0.0001 ***P < 0.001 **P < 0.01 versus sham-operated mice, ####P < 0.001 ###P < 0.01 versus BCAS-operated Cx43^{+/+} mice, n ≥ 6 mice for each group.

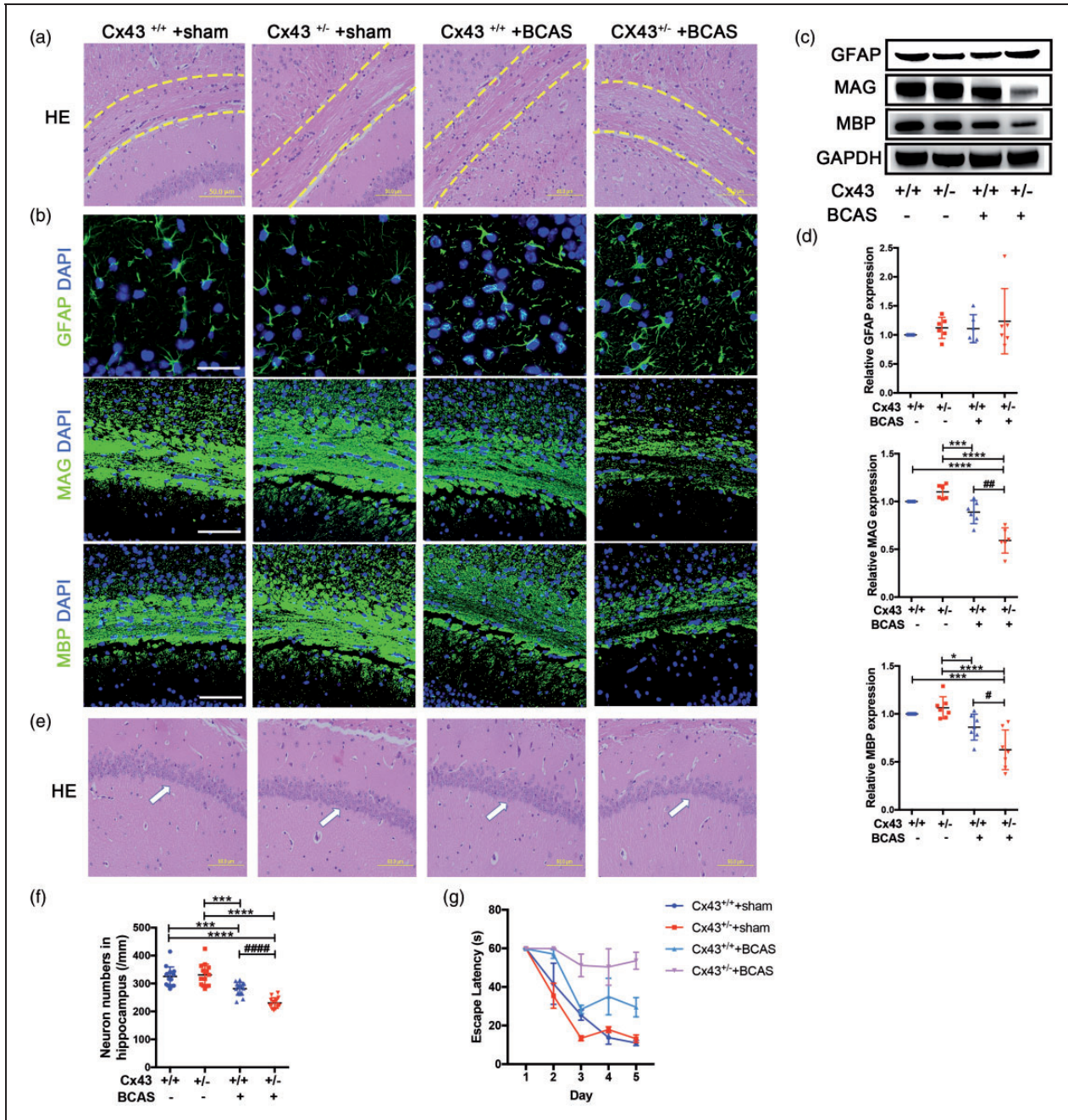


Figure 4. Representative images to explicate the pathogenesis of white matter and hippocampal neuron injury in Cx43 WT and KO mice. (a) HE staining was used to observe the changes in WMLs in CC (critical areas indicated between two yellow dotted lines) of sham- and BCAS-operated mice. Scale bar = 50 μm. (b) Representative images depicting immunofluorescent labeling of GFAP, MAG and MBP with DAPI in mouse CC, which are indicative of a loss of myelin integrity and damage. Scale bar = 100 μm. (c) Western blot analysis for GFAP, MAG and MBP expression with GAPDH used as an internal control. (d) Quantitative analysis of proteins relative to GAPDH was performed. (e) The results of HE staining also showed significant damage in hippocampal neurons (white arrows). Scale bar = 50 μm. (f) Quantification of the hippocampal CA1 neurons for the Morris water maze. The escape latency during training was recorded and analyzed. ****P < 0.0001 ***P < 0.001 *P < 0.05 versus sham-operated mice, #####P < 0.0001 ###P < 0.01 #P < 0.05 versus BCAS-operated Cx43^{+/+} mice, n ≥ 6 mice for each group.

p-AKT levels were obviously higher in BCAS-operated Cx43^{+/+} mice compared to sham-operated mice and BCAS-operated Cx43^{+/-} mice. No statistical difference of p-AKT levels was observed between BCAS-operated Cx43^{+/-} mice and sham-operated mice (Figure S2(a) and (b)). HIF-1 α /PAK pathway remained active until 30 days after surgery (Figure 5(a) and (b)). We next separately analyzed HIF-1 α /p-AKT pathway in the cortex and white matter 30 days after surgery, and the results demonstrate that the HIF-1 α /p-AKT pathway was equally important for the cortex and white matter (Figure 5(c) and (d)). Additionally, we analyzed the mRNA expression of HIF-1 α and VEGF. The results showed that the mRNA expression of HIF-1 α and VEGF in brains were both significantly upregulated in BCAS-operated Cx43^{+/+} mice compared to Cx43^{+/-} mice (Figure 5(e) and (f)). These results indicate that Cx43 may mediate VEGF-induced angiogenesis in an HIF-1 α -dependent manner, and that p-AKT plays a major role in regulating the HIF-1 α /VEGF pathway.

Cx43 mediates angiogenesis and tight junction disruption in a hypoxic environment induced by CoCl₂ in vitro

The bEnd.3 cells were treated with Cx43 siRNA to reduce the expression of Cx43 and western blot results indicated that the Cx43 expression was downregulated approximately 4 fold (Figure 6(a) and (b)). CoCl₂, a hypoxia-mimetic agent *in vitro*, inhibits prolyl-hydroxylase enzymes, contributing to the accumulation of HIF-1 α .⁵⁵ bEnd.3 cells were incubated with 0–500 μ M CoCl₂ for 24 h.⁵⁶ As shown in Figure 6(c), CoCl₂ levels of 375 μ M and 500 μ M led to significant upregulation of HIF-1 α by approximately 6 and 7 fold (Figure 6(c) and (d)). In addition, cells were subjected to a CCK-8 assay to evaluate cell viability. The CCK-8 readings from CoCl₂-treated groups were compared with the control group (no CoCl₂ treatment). We found that the viability of cells treated with 375 μ M and 500 μ M of CoCl₂ showed significant changes compared to the control cells (Figure 6(e); 375 μ M 77.6 \pm 3.987%, 500 μ M 73.68 \pm 3.987%). We chose 375 μ M as the final CoCl₂ concentration because there were already significant group differences at this level. To study the angiogenic response in Cx43-deficient bEnd.3 cells, we measured the migratory ability of Cx43-deficient ECs and found it was significantly decreased compared with control cells (Figure 6(f)). Quantitative analysis of the migratory areas revealed that for bEnd.3 ECs the area was about 9 fold higher than Cx43-deficient ECs under CoCl₂ treatment (Figure 6(g)). These results indicate that Cx43 deficiency impairs endothelial angiogenesis in response to CoCl₂-induced chronic hypoxia.

To verify whether barrierogenesis happens simultaneously with EC angiogenesis using an *in vitro* model of CoCl₂, immunofluorescence staining and western blotting were used to examine endothelial barrier function. Immunofluorescence staining for ZO-1 (red) and claudin-5 (red) revealed reduced expression in siRNA-treated cells compared with NC-treated cells exposed to CoCl₂ (Figure 6(h)). Additionally, levels of claudin-5 (P=0.039) and ZO-1 (P=0.011) were significantly decreased in siRNA-treated cells compared with NC-treated cells under CoCl₂ treatment (Figure 6(i) and (j)). These results suggest that angiogenesis disorder caused by Cx43 deficiency is accompanied with the impaired integrity of endothelial barrier, characterized by the reduced tight junction (TJ) proteins.

Cx43 promotes the VEGF-induced angiogenesis in a HIF-1 α dependent manner in vitro

To assess the secretion of VEGF from bEnd.3 cells, we performed an ELISA assay of the culture medium. VEGF release was clearly elevated in CoCl₂-treated cells compared with cells without CoCl₂ treatment, while VEGF secretion in NC-treated cells was approximately 2 fold that of siRNA-treated cells under CoCl₂ (Figure 7(a)). RT-PCR results showed that HIF-1 α mRNA expression in siRNA-treated cells was reduced compared with NC-treated cells under CoCl₂ stimulation (Figure 7(b)). These results support the conclusion that Cx43 can upregulate HIF-1 α expression *in vitro*. The results of RT-PCR demonstrated VEGF mRNA expression levels were consistent with the VEGF ELISA assay. VEGF mRNA was upregulated in cells after exposure to CoCl₂ for 24 h and VEGF mRNA levels in siRNA-treated cells were significantly lower than in NC-treated cells (Figure 7(c)). The VEGF overexpression induced by hypoxia was eliminated by Cx43 deficiency. Additionally, we verified the effects upstream of VEGF, including HIF-1 α and AKT signaling pathways, *in vitro* by western blotting. Consistent with the findings *in vivo*, the downregulation of Cx43 by siRNA significantly reduced HIF-1 α (P < 0.0001) and p-AKT (P = 0.03) expression compared to NC-treated cells under CoCl₂ treatment but did not affect AKT expression (Figure 7(d) and (e)). To further confirm that Cx43 mediates VEGF-induced angiogenesis in a HIF-1 α dependent manner, we overexpressed HIF-1 α in the Cx43 deficient cells via lentivirus transfection as described in the Materials and Methods section. We first confirmed the transfection efficiency in bEnd.3 cells by western blot analysis. The result showed that HIF-1 α expression in JLV-HIF-1 α -treated cells was approximately 1.6 fold that of NC-treated cells (Figure 7(f) to (g)). Subsequently, we compared the activation of the PKA signaling pathway and

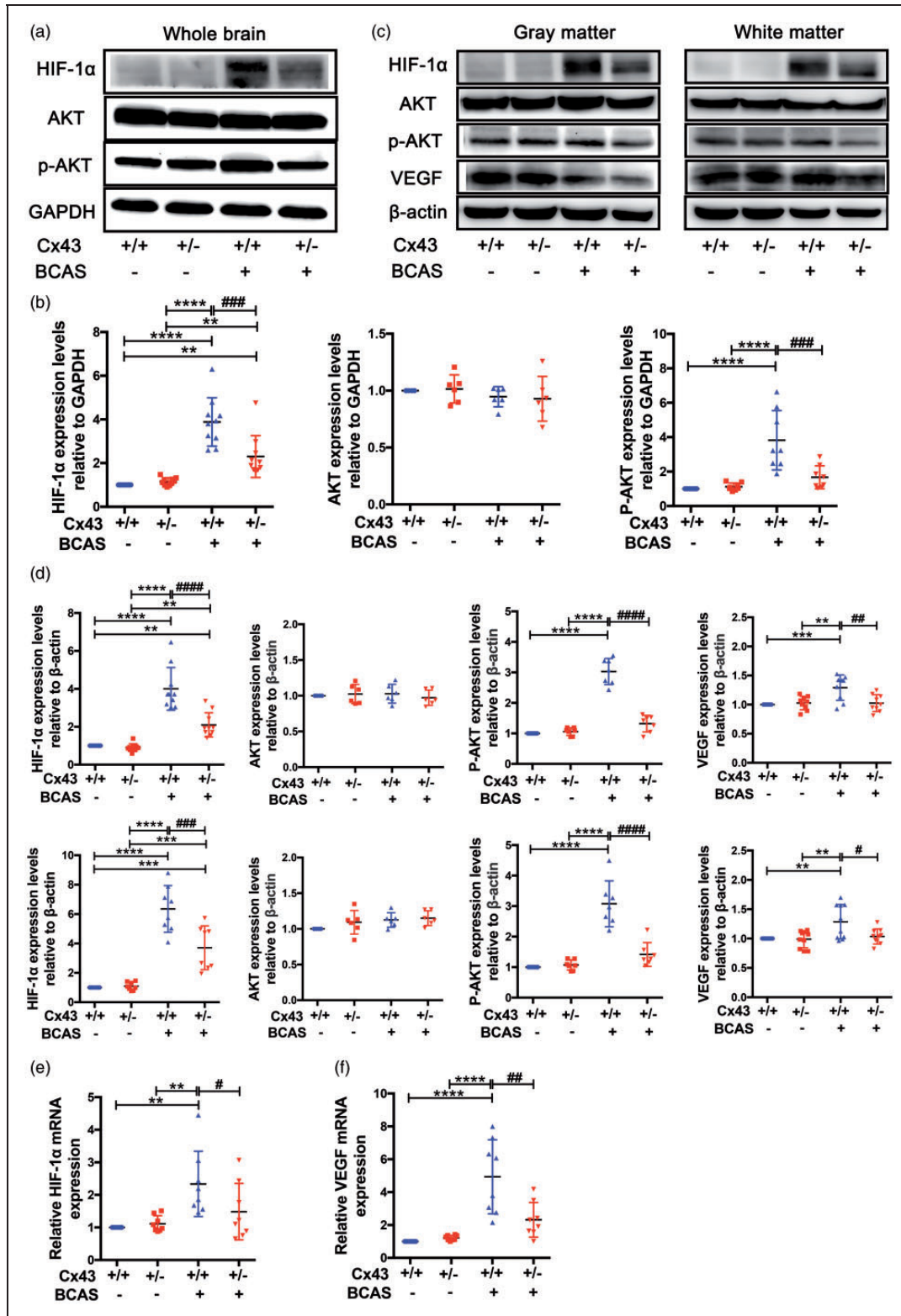


Figure 5. Cx43 regulated VEGF-induced angiogenesis through the HIF-1 α -PKA signaling pathway. The brain tissues removed from the four mouse groups 30 days after surgery were used for western blots and RT-PCR. (a) Representative images of western blots for HIF-1 α , AKT, and p-AKT using GAPDH as an internal control. (b) Differences in the band intensities of HIF-1 α , AKT, and p-AKT were compared among the four mouse groups. (c) Representative images of separate western blot analyses for the HIF-1 α /P-AKT pathway in white and gray matter using β -actin as an internal control. (d) Quantitative analysis of the band intensities relative to β -actin. (e) HIF-1 α mRNA expression in the four mouse groups was evaluated using RT-PCR. (f) RT-PCR measures of VEGF mRNA in each group of mice. **** $P < 0.0001$ *** $P < 0.001$ ** $P < 0.01$ versus sham-operated mice, ##### $P < 0.00001$ #### $P < 0.0001$ ### $P < 0.01$ # $P < 0.05$ versus BCAS-operated Cx43^{+/+} mice, $n \geq 6$ mice for each group.

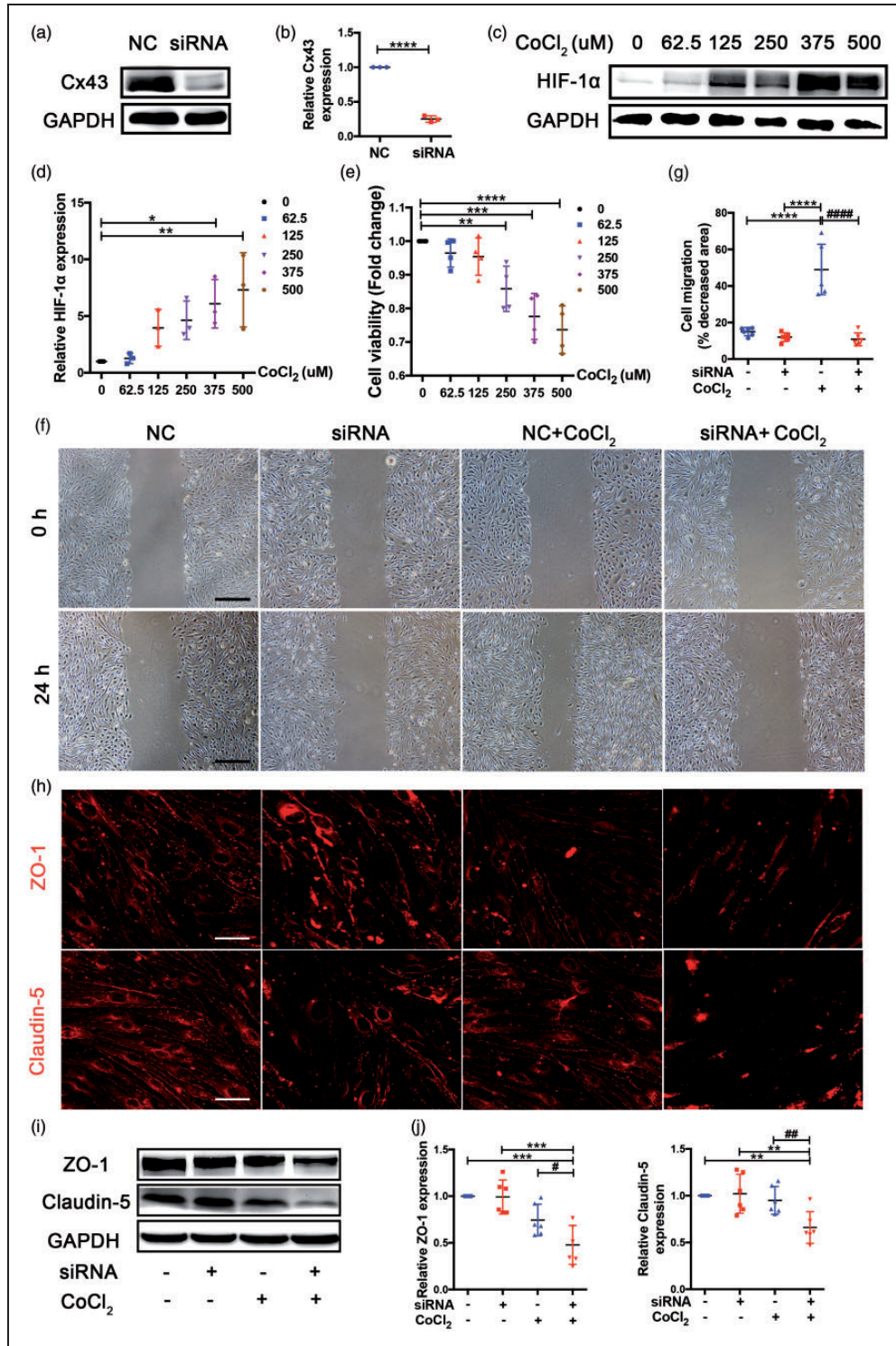


Figure 6. Cx43-deficient bEnd.3 cells were defective in the migration involved in angiogenesis and TJ protein levels. (a) Western blot analysis of Cx43 expression in NC and siRNA-treated bEnd.3 cells. (b) Quantitative analysis of Cx43 protein level relative to GAPDH. (c) Western blot analysis for HIF-1α extracted from bEnd.3 cells treated with 0, 62.5, 125, 250, 375, and 500 μmol/L CoCl₂ for 24 h to select the suitable hypoxic concentration, and GAPDH was an internal control. (d) Quantitative analysis of HIF-1α level relative to GAPDH. (e) CCK-8 assay was used to assess cell viability. The CCK-8 readings further contributed to choosing the suitable hypoxic concentration. (f) Representative images of endothelial wound healing assay. Scale bar = 0.5 mm. (g) Quantitative analysis of migratory area expressed as pixels squared. (h) Representative images depicting immunofluorescent labeling claudin-5 and ZO-1 in the four cell groups. Scale bar = 100 μm. (i) Western blot analysis for claudin-5 and ZO-1 of samples from the four group bEnd.3 cell groups. (j) Quantitative analysis of claudin-5 and ZO-1 relative to GAPDH was performed. ****P < 0.0001 ***P < 0.001 **P < 0.01 *P < 0.05 versus control cells, #####P < 0.0001 ###P < 0.01 #P < 0.05 versus CoCl₂-treated control cells. All these studies were conducted independently at least three times.

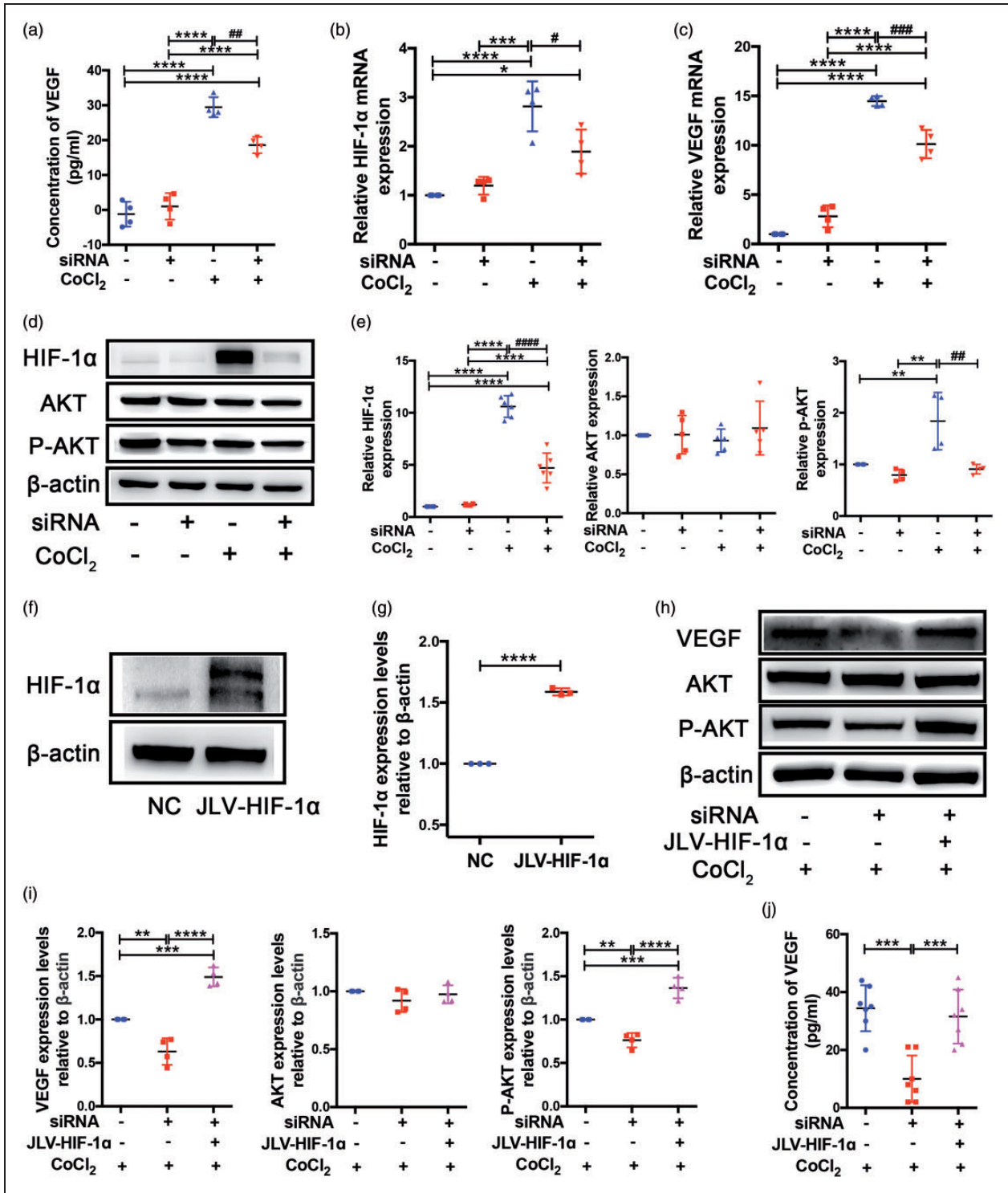


Figure 7. Cx43 mediated VEGF-induced angiogenesis by activating the HIF-1 α -PKA signaling pathway *in vitro*. (a) VEGF contents in the culture medium of each group of cells were analyzed using a VEGF ELISA kit. (b) HIF-1 α mRNA expression in four cell groups were studied by RT-PCR. (c) RT-PCR results indicating VEGF mRNA levels in each cell group. (d) Western blot images of HIF-1 α , AKT, and p-AKT from the cultured bEnd.3 samples in four difference groups. β -actin was an internal control. (e) Quantitative analysis of protein levels relative to β -actin. (f) Western blot analysis of HIF-1 α expression in lentivirus-transfected cells. (g) Quantitative analysis of HIF-1 α protein level relative to β -actin. (h) Representative images of western blots for VEGF, AKT, and p-AKT expression in the three group bEnd.3 cell groups treated with 375 μ mol/L CoCl₂ for 24 h. (i) Quantitative analysis of the band intensities relative to β -actin. (j) VEGF concentrations in the culture medium of the three group bEnd.3 cell groups were analyzed using a VEGF ELISA kit. ****P < 0.0001 ***P < 0.001 **P < 0.01 *P < 0.05 versus control cells, #####P < 0.0001 ####P < 0.001 ###P < 0.01 #P < 0.05 versus CoCl₂-treated control cells. All these studies were conducted independently at least three times.

VEGF expression using western blot analysis for the three groups of CoCl₂-treated cells: NC, Cx43 siRNA, and Cx43 siRNA + JLV-HIF-1 α . The results indicated that HIF-1 α overexpression in the Cx43 deficient cells can reverse the expression of VEGF via the PKA signaling pathway (Figure 7(h) to (i)). Additionally, we performed an ELISA assay of the culture medium to assess the VEGF secretion in the three groups of cells and the result was consistent with western blot analysis of VEGF (Figure 7(j)). Therefore, it is reasonable to conclude that Cx43 mediates HIF-1 α expression and subsequently promotes VEGF-induced angiogenesis through the PKA signaling pathway.

Discussion

In the current study, we explored the role of Cx43 in promoting angiogenesis during CCH using *in vivo* and *in vitro* models. We demonstrated four major findings. First, Cx43 mediated VEGF-induced reparative angiogenesis in a chronic hypoxic environment both *in vivo* and *in vitro*. Second, Cx43 mediated HIF-1 α expression to activate the PKA signaling pathway, which is required for VEGF-induced angiogenesis. Third, BBB integrity was simultaneously improved accompanied by Cx43-mediated angiogenesis. Finally, the pathogenesis of WMLs and neuronal injury after CCH could be ameliorated by Cx43-promoted angiogenesis and improved BBB integrity. These findings are important for developing clinical responses to CCH because a thorough understanding of the signaling mechanisms underlying Cx43-induced angiogenesis is critical for directing new therapeutic strategies that can affect the early stages of CCH-induced diseases in humans.

Angiogenesis is the process of forming new blood vessels from existing vascular networks, and it can be both a normal physiological phenomenon and a pathological response to CNS disease progression.⁵⁷ It is well acknowledged that angiogenesis is a complicated process involving various cytokines in the endothelium, growth factors and extracellular matrix (ECM) molecules. However, VEGF is largely the focus of mechanistic and inhibitor studies.⁵⁸ Besides involving indirect cell-cell communication through various growth factors in endothelium, angiogenesis can also be mediated by direct cell-cell junctions, such as GJs,⁵⁹ which are responsible for GJIC between the coupled cells.⁶⁰ Currently, several studies indicate that Cx43 GJs can mediate angiogenesis in some tissues.^{29,30,61} However, there is controversy about the role of Cx43 GJs in angiogenesis. It is interesting that Cx43 GJs also can inhibit angiogenesis by transferring anti-angiogenic microRNAs from microvascular ECs to cancer cells.⁶¹ Controversy over the role of Cx43 in angiogenesis might be due to variability in the molecular

substances transferred via Cx43 GJs under different pathological conditions and in different tissues. Additionally, although the role of Cx43 in angiogenesis is controversial, the ultimate effect of Cx43 on angiogenesis is beneficial for normal physiology. Few articles to date have addressed the effect of Cx43 on cerebral microangiogenesis in the context of CCH. In our study, we demonstrated that Cx43 promotes cerebral angiogenesis in a chronic hypoxic environment by increasing the VEGF level, which plays an essential role in angiogenesis,⁶² and this finding is consistent with previous reports.²⁸

Furthermore, we demonstrated that Cx43 mediates VEGF-induced angiogenesis in a HIF-1 α -dependent manner under CCH, which is equally important for the cortex and white matter. Although the HIF-1 α /VEGF pathway has already been identified as relevant in range of hypoxia-related diseases in the heart,⁶³ hindlimb,⁶⁴ kidney⁶⁵ and especially in tumors,^{66,67} it has rarely been reported on in the context of CCH diseases. Additionally, the relationship between Cx43 and HIF-1 α has not been well-specified. We have not only demonstrated that Cx43 can promote angiogenesis by up-regulating HIF-1 α expression but also determined that the PKA signaling pathway is involved in Cx43-induced HIF-1 α expression. This is consistent with previous studies which have reported that the PKA pathway is essential for HIF-1 α /VEGF activation under hypoxic conditions.⁶⁸ Cx43-mediated HIF-1 α /VEGF pathway can be activated at 7 days under hypoxic conditions and last until 30 days after the BCAS surgery. However, the levels of upregulated proteins in HIF-1 α /VEGF pathway at 30 days were relatively lower than that at 7 days, which might be due to the partial recovery of CBF at 30 days in BCAS-operated Cx43^{+/+} mice. Additionally, the expression and activity of HIF-1 α can be modulated through related signaling pathways in addition to being induced in response to reduced oxygen availability.⁶⁹ In addition to the AKT pathway signaling mentioned in our study, the extracellular signal-regulated kinase (ERK) pathway has also been identified as a major signaling pathway.⁷⁰ Both the ERK and AKT pathways play characteristic roles in governing growth, proliferation, differentiation and survival in most cells. However, it remains a mystery whether the ERK pathway participates in the signaling of HIF-1 α /VEGF activation mediated by Cx43 under CCH, so further investigation is required to examine this possibility.

Ischemic diseases caused by the insufficient supply of oxygen and nutrients in the blood are the major causes of disabilities and deaths. Previous studies have indicated that angiogenesis is beneficial for improving blood flow and function in animal models of ischemic diseases.^{33,71} CCH, caused by various

etiologies, has been considered to be difficult to use a single unified hypothesis to conclusively explain all distinctive features and associated with the development of VCID.⁷² Notably, although age is a key risk factor for the development of VCID, most studies still use relatively young rodents (10-12 weeks) due to the fact that endogenous remodeling mechanisms can be more efficient in young rodents and CCH mouse model induced by BCAS demonstrates good reproducibility in terms of the characteristic damage of VCID in young mice including WMLs and cognitive impairment.^{73,74} In our study, we identified the characteristic pathophysiology of vascular dementia in BCAS-operated Cx43^{+/-} mice with poor angiogenesis. Our findings suggest that Cx43-mediated angiogenesis decreases the pathological changes in VCID induced by CCH. The medical treatment for VCID has attracted extensive attention and various compounds with different mechanisms are used in treatment, but they have only mild efficacy⁷⁵ and no drug has demonstrated the potential to arrest the progress of VCID. A thorough understanding of the signaling mechanisms underlying the molecules and pathways upstream of VEGF-induced angiogenesis could provide vital tools to develop interventions that can ameliorate brain damage at the early stages. We suggest that Cx43-related angiogenesis is a promising therapeutic target for attenuating the pathological changes in VCID caused by CCH, and potentially other ischemic diseases. Recently, specific microRNAs have been believed to be involved in the possible molecular mechanisms and signaling pathways of VCID pathophysiology.⁷⁶ Interestingly, previous study have demonstrated that Cx43-mediated GJIC can affect the angiogenesis of tumor via transferring microRNA from endothelial cells to tumor cells.⁶¹ These valuable discoveries can provide another possible research direction for Cx43 in the VCID pathophysiology.

Our findings suggest the following sequence of events: impaired angiogenesis due to Cx43 deficiency initiates microcirculatory insufficiency and BBB disruption first, followed by the secondary neurodegenerative changes characteristic of VCID. These results suggest a novel vascular mechanism underpinning VCID, which is critical for our understanding of how VCID is caused by CCH and may be instructive for new therapeutic methods. Notably, previous studies have revealed a significant increase of Evans blue densities in the brains of BCAS mice on day 3.⁵¹ However, 3 days post-surgery, the western blot analysis of tight junctions including ZO-1 and claudin-5 demonstrated no difference among four group mice (Figure S3(a) and (b)), which is consistent with the prior research.⁷⁷ This phenomenon may be related to the possibility that Evans blue crosses the BBB via a transendothelial

rather than a paracellular pathway. Additionally, there are still some limitations in this study. Mice with global Cx43 homozygous deficiency cannot be used because they die perinatally owing to an obstruction of the right ventricular outflow tract of the heart.⁷⁸ ECs in Cx43 heterozygous mice still express some amount of Cx43 protein. Additionally, Cx43 protein is also expressed in other cell types such as vascular smooth muscle cells, pericytes and astrocytes.⁷⁹ Thus, further research is needed to understand the influence of Cx43-deficiency on angiogenesis in these type of cells. In particular, the use of endothelium-specific Cx43 knockout mice and the primary microvascular endothelial cells obtained from endothelium-specific Cx43 knockout mice could be helpful to validate the results of our study.

Funding

The authors disclosed receipt of the following financial support for the research, authorship, and/or publication of this article: This work was supported by the National Natural Science Foundation of China [NSFC: 8,19,71,115] and National Science and Technology Major Project [2017ZX09304028].

Acknowledgements

The authors appreciate the technical support provided by Professor Lemin Zheng. The authors would like to thank Professor Jinyan Han for providing the Laser Doppler perfusion image system to measure cerebral brain flow. The authors appreciate the MRA support from Chinese Academy of Sciences-Institute of Automation, Center for Advanced Imaging.

Declaration of conflicting interests

The author(s) declared no potential conflicts of interest with respect to the research, authorship, and/or publication of this article.

Authors' contributions

Weiwei Yu was involved in the conceptualization and design of this study, analyzing and interpreting these data, and drafting and revising the this manuscript. Haiqiang Jin was involved in designing the study and revising the manuscript. Wei Sun was involved in revising the manuscript and obtained funding. Ding Nan was involved in analyzing the data and revising the manuscript. Jianwen Deng contributed toward analyzing and interpreting the data, and revising the manuscript. Jingjing Jia was involved in designing the *in vitro* cellular experiments and analyzing the data. Zemou Yu was involved in the analysis and interpretation of the data. Yining Huang participated in the conceptualization and design of the study, and revising the manuscript, and obtaining funding.

Supplementary material

Supplemental material for this article is available online.

ORCID iDYining Huang  <https://orcid.org/0000-0002-1657-4151>**References**

- Kalaria RN. Neuropathological diagnosis of vascular cognitive impairment and vascular dementia with implications for Alzheimer's disease. *Acta Neuropathol* 2016; 131: 659–685.
- Wallin A, Roman GC, Esiri M, et al. Update on vascular cognitive impairment associated with subcortical small-vessel disease. *J Alzheimers Dis* 2018; 62: 1417–1441.
- Yu P, Venkat P, Chopp M, et al. Role of microRNA-126 in vascular cognitive impairment in mice. *J Cereb Blood Flow Metab* 2019; 39: 2497–2511.
- Toth P, Tarantini S, Csiszar A, et al. Functional vascular contributions to cognitive impairment and dementia: mechanisms and consequences of cerebral autoregulatory dysfunction, endothelial impairment, and neurovascular uncoupling in aging. *Am J Physiol Heart Circ Physiol* 2017; 312: H1–h20.
- Paulson OB, Hasselbalch SG, Rostrup E, et al. Cerebral blood flow response to functional activation. *J Cereb Blood Flow Metab* 2010; 30: 2–14.
- de la Torre JC, Olmo AD and Valles S. Can mild cognitive impairment be stabilized by showering brain mitochondria with laser photons? *Neuropharmacology* 2020; 171: 107841.
- Hooghiemstra AM, Leeuwis AE, Bertens AS, et al. Frequent cognitive impairment in patients with disorders along the heart-brain axis. *Stroke* 2019; 50: 3369–3375.
- Love S and Miners JS. Small vessel disease, neurovascular regulation and cognitive impairment: post-mortem studies reveal a complex relationship, still poorly understood. *Clin Sci* 2017; 131: 1579–1589.
- De Silva TM and Faraci FM. Microvascular dysfunction and cognitive impairment. *Cell Mol Neurobiol* 2016; 36: 241–258.
- Iadecola C. The overlap between neurodegenerative and vascular factors in the pathogenesis of dementia. *Acta Neuropathol* 2010; 120: 287–296.
- Jellinger KA. Pathology and pathogenesis of vascular cognitive impairment—a critical update. *Front Aging Neurosci* 2013; 5: 17.
- Deramecourt V, Slade JY, Oakley AE, et al. Staging and natural history of cerebrovascular pathology in dementia. *Neurology* 2012; 78: 1043–1050.
- Rosenberg GA. Neurological diseases in relation to the blood-brain barrier. *J Cereb Blood Flow Metab* 2012; 32: 1139–1151.
- Moorer MC and Stains JP. Connexin43 and the intercellular signaling network regulating skeletal remodeling. *Curr Osteoporos Rep* 2017; 15: 24–31.
- Kikuchi-Taura A, Okinaka Y, Takeuchi Y, et al. Bone marrow mononuclear cells activate angiogenesis via gap junction-mediated cell-cell interaction. *Stroke* 2020; 51: 1279–1289.
- Alexander DB and Goldberg GS. Transfer of biologically important molecules between cells through gap junction channels. *Curr Med Chem* 2003; 10: 2045–2058.
- Goodenough DA, Goliger JA and Paul DL. Connexins, connexons, and intercellular communication. *Annu Rev Biochem* 1996; 65: 475–502.
- Laird DW. Life cycle of connexins in health and disease. *Biochem J* 2006; 394: 527–543.
- Sohl G and Willecke K. An update on connexin genes and their nomenclature in mouse and man. *Cell Commun Adhes* 2003; 10: 173–180.
- Rovegno M and Saez JC. Role of astrocyte connexin hemichannels in cortical spreading depression. *Biochim Biophys Acta Biomembr* 2018; 1860: 216–223.
- Nagy JI, Dudek FE and Rash JE. Update on connexins and gap junctions in neurons and glia in the mammalian nervous system. *Brain Res Brain Res Rev* 2004; 47: 191–215.
- Giaume C and Theis M. Pharmacological and genetic approaches to study connexin-mediated channels in glial cells of the Central nervous system. *Brain Res Rev* 2010; 63: 160–176.
- Giaume C, Koulakoff A, Roux L, et al. Astroglial networks: a step further in neuroglial and gliovascular interactions. *Nat Rev Neurosci* 2010; 11: 87–99.
- Freitas-Andrade M, She J, Bechberger J, et al. Acute connexin43 temporal and spatial expression in response to ischemic stroke. *J Cell Commun Signal* 2018; 12: 193–204.
- Yi C, Mei X, Ezan P, et al. Astroglial connexin43 contributes to neuronal suffering in a mouse model of Alzheimer's disease. *Cell Death Differ* 2016; 23: 1691–1701.
- Kawasaki A, Hayashi T, Nakachi K, et al. Modulation of connexin 43 in rotenone-induced model of Parkinson's disease. *Neuroscience* 2009; 160: 61–68.
- Deshpande T, Li T, Herde MK, et al. Subcellular reorganization and altered phosphorylation of the astrocytic gap junction protein connexin43 in human and experimental temporal lobe epilepsy. *Glia* 2017; 65: 1809–1820.
- Wang HH, Su CH, Wu YJ, et al. Reduction of connexin43 in human endothelial progenitor cells impairs the angiogenic potential. *Angiogenesis* 2013; 16: 553–560.
- Liu C, Fan Y, Zhou L, et al. Pretreatment of mesenchymal stem cells with angiotensin II enhances paracrine effects, angiogenesis, gap junction formation and therapeutic efficacy for myocardial infarction. *Int J Cardiol* 2015; 188: 22–32.
- Li H, He J, Yu H, et al. Bioglass promotes wound healing by affecting gap junction connexin 43 mediated endothelial cell behavior. *Biomaterials* 2016; 84: 64–75.
- Wang M, Qin C, Luo X, et al. Astrocytic connexin 43 potentiates myelin injury in ischemic white matter disease. *Theranostics* 2019; 9: 4474–4493.
- Wang GL, Jiang BH, Rue EA, et al. Hypoxia-inducible factor 1 is a basic-helix-loop-helix-PAS heterodimer regulated by cellular O₂ tension. *Proc Natl Acad Sci U S A* 1995; 92: 5510–5514.
- Li M, Cui Y, He W, et al. Effects of triple-mutated hypoxia-inducible factor-1alpha on angiogenesis and cardiac function improvement in rats with myocardial infarction. *Cell Physiol Biochem* 2018; 50: 2329–2340.

34. Semenza GL. Oxygen sensing, hypoxia-inducible factors, and disease pathophysiology. *Annu Rev Pathol* 2014; 9: 47–71.
35. Wan J and Wu W. Hyperthermia induced HIF-1 α expression of lung cancer through AKT and ERK signaling pathways. *J Exp Clin Cancer Res* 2016; 35: 119.
36. Sun Y, Chen X, Zhang X, et al. beta2-adrenergic receptor-mediated HIF-1 α upregulation mediates blood brain barrier damage in acute cerebral ischemia. *Front Mol Neurosci* 2017; 10: 257.
37. Percie Du Sert N, Hurst V, Ahluwalia A, et al. The ARRIVE guidelines 2.0: updated guidelines for reporting animal research. *J Cereb Blood Flow Metab* 2020; 40: 1769–1777.
38. Lee ES, Yoon JH, Choi J, et al. A mouse model of subcortical vascular dementia reflecting degeneration of cerebral white matter and microcirculation. *J Cereb Blood Flow Metab* 2019; 39: 44–57.
39. Mao XW, Pan CS, Huang P, et al. Levo-tetrahydropalmatine attenuates mouse blood-brain barrier injury induced by focal cerebral ischemia and reperfusion: involvement of src kinase. *Sci Rep* 2015; 5: 11155.
40. Chen FQ, Li Q, Pan CS, et al. Kudiezi injection((R)) alleviates blood-brain barrier disruption after Ischemia-Reperfusion in rats. *Microcirculation* 2016; 23: 426–437.
41. Paris D, Quadros A, Humphrey J, et al. Nilvadipine antagonizes both abeta vasoactivity in isolated arteries, and the reduced cerebral blood flow in APPsw transgenic mice. *Brain Res* 2004; 999: 53–61.
42. Aguilera KY and Brekken RA. Hypoxia studies with pimonidazole in vivo. *Bio Protoc* 2014; 4: e1254.
43. Zhu D, Wang Y, Singh I, et al. Protein S controls hypoxic/ischemic blood-brain barrier disruption through the TAM receptor Tyro3 and sphingosine 1-phosphate receptor. *Blood* 2010; 115: 4963–4972.
44. Meijering E, Jacob M, Sarria JC, et al. Design and validation of a tool for neurite tracing and analysis in fluorescence microscopy images. *Cytometry A* 2004; 58: 167–176.
45. Miyamoto N, Pham LD, Hayakawa K, et al. Age-related decline in oligodendrogenesis retards white matter repair in mice. *Stroke* 2013; 44: 2573–2578.
46. Li X, Liu C, Li P, et al. Connexin 43 is a potential regulator in fluid shear stress-induced signal transduction in osteocytes. *J Orthop Res* 2013; 31: 1959–1965.
47. Huang GY, Xie LJ, Linask KL, et al. Evaluating the role of connexin43 in congenital heart disease: screening for mutations in patients with outflow tract anomalies and the analysis of knock-in mouse models. *J Cardiovasc Dis Res* 2011; 2: 206–212.
48. Ihara M, Taguchi A, Maki T, et al. A mouse model of chronic cerebral hypoperfusion characterizing features of vascular cognitive impairment. *Methods Mol Biol* 2014; 1135: 95–102.
49. Umans RA, Henson HE, Mu F, et al. CNS angiogenesis and barrierogenesis occur simultaneously. *Dev Biol* 2017; 425: 101–108.
50. Engelhardt B and Liebner S. Novel insights into the development and maintenance of the blood-brain barrier. *Cell Tissue Res* 2014; 355: 687–699.
51. Liu Q, Radwanski R, Babadjouni R, et al. Experimental chronic cerebral hypoperfusion results in decreased pericyte coverage and increased blood-brain barrier permeability in the corpus callosum. *J Cereb Blood Flow Metab* 2019; 39: 240–250.
52. Ma J, Bo SH, Lu XT, et al. Protective effects of carnosine on white matter damage induced by chronic cerebral hypoperfusion. *Neural Regen Res* 2016; 11: 1438–1444.
53. Belaiba RS, Bonello S, Zahringer C, et al. Hypoxia upregulates hypoxia-inducible factor-1 α transcription by involving phosphatidylinositol 3-kinase and nuclear factor kappaB in pulmonary artery smooth muscle cells. *Mol Biol Cell* 2007; 18: 4691–4697.
54. Chi ZL, Adini A, Birsner AE, et al. PR1P ameliorates neurodegeneration through activation of VEGF signaling pathway and remodeling of the extracellular environment. *Neuropharmacology* 2019; 148: 96–106.
55. Li S, Zhang J, Yang H, et al. Copper depletion inhibits CoCl₂-induced aggressive phenotype of MCF-7 cells via downregulation of HIF-1 and inhibition of snail/twist-mediated epithelial-mesenchymal transition. *Sci Rep* 2015; 5: 12410.
56. Wu D and Yotnda P. Induction and testing of hypoxia in cell culture. *J Vis Exp* 2011; 54: 2899.
57. Vallon M, Chang J, Zhang H, et al. Developmental and pathological angiogenesis in the central nervous system. *Cell Mol Life Sci* 2014; 71: 3489–3506.
58. Ronca R, Benkheil M, Mitola S, et al. Tumor angiogenesis revisited: regulators and clinical implications. *Med Res Rev* 2017; 37: 1231–1274.
59. Okamoto T, Usuda H, Tanaka T, et al. The functional implications of endothelial gap junctions and cellular mechanics in vascular angiogenesis. *Cancers* 2019; 11: 237.
60. Zhou JZ and Jiang JX. Gap junction and hemichannel-independent actions of connexins on cell and tissue functions—an update. *FEBS Lett* 2014; 588: 1186–1192.
61. Thuringer D, Jago G, Berthenet K, et al. Gap junction-mediated transfer of miR-145-5p from microvascular endothelial cells to Colon cancer cells inhibits angiogenesis. *Oncotarget* 2016; 7: 28160–28168.
62. Zhou PT, Wang LP, Qu MJ, et al. DI-3-N-butylphthalide promotes angiogenesis and upregulates sonic hedgehog expression after cerebral ischemia in rats. *CNS Neurosci Ther* 2019; 25: 748–758.
63. Mirzaei BF, Karimi-Sales E, Alihemmati A, et al. Effect of ghrelin on hypoxia-related cardiac angiogenesis: involvement of miR-210 signalling pathway. *Arch Physiol Biochem* 2019; 9: 1–6.
64. Zheng J, Chen M, Ye C, et al. BuZangTongLuo decoction improved hindlimb ischemia by activating angiogenesis and regulating gut microbiota in diabetic mice. *J Ethnopharmacol* 2020; 248: 112330.
65. Bessho R, Takiyama Y, Takiyama T, et al. Hypoxia-inducible factor-1 α is the therapeutic target of the SGLT2 inhibitor for diabetic nephropathy. *Sci Rep* 2019; 9: 14754.
66. Zhang B, Huang X, Wang H, et al. Promoting antitumor efficacy by suppressing hypoxia via nano self-assembly of

- two irinotecan-based dual drug conjugates having a HIF-1 α inhibitor. *J Mater Chem B* 2019; 7: 5352–5362.
67. Wan J, Ma J, Mei J, et al. The effects of HIF-1 α on gene expression profiles of NCI-H446 human small cell lung cancer cells. *J Exp Clin Cancer Res* 2009; 28: 150.
68. Sun YZ, Cai N and Liu NN. Celecoxib down-regulates the hypoxia-induced expression of HIF-1 α and VEGF through the PI3K/AKT pathway in retinal pigment epithelial cells. *Cell Physiol Biochem* 2017; 44: 1640–1650.
69. Zhang QL, Cui BR, Li HY, et al. MAPK and PI3K pathways regulate hypoxia-induced atrial natriuretic peptide secretion by controlling HIF-1 α expression in beating rabbit atria. *Biochem Biophys Res Commun* 2013; 438: 507–512.
70. Agani F, and Jiang BH. Oxygen-independent regulation of HIF-1: novel involvement of PI3K/AKT/mTOR pathway in cancer. *Curr Cancer Drug Targets* 2013; 13: 245–251.
71. Manuel GE, Johnson T and Liu D. Therapeutic angiogenesis of exosomes for ischemic stroke. *Int J Physiol Pathophysiol Pharmacol* 2017; 9: 188–191.
72. Zhou D, Meng R, Li SJ, et al. Advances in chronic cerebral circulation insufficiency. *CNS Neurosci Ther* 2018; 24: 5–17.
73. Duncombe J, Kitamura A, Hase Y, et al. Chronic cerebral hypoperfusion: a key mechanism leading to vascular cognitive impairment and dementia. Closing the translational gap between rodent models and human vascular cognitive impairment and dementia. *Clin Sci* 2017; 131: 2451–2468.
74. Kalaria RN. The pathology and pathophysiology of vascular dementia. *Neuropharmacology* 2018; 134: 226–239.
75. Baskys A and Cheng JX. Pharmacological prevention and treatment of vascular dementia: approaches and perspectives. *Exp Gerontol* 2012; 47: 887–891.
76. Zhang J, Sun P, Zhou C, et al. Regulatory microRNAs and vascular cognitive impairment and dementia. *CNS Neurosci Ther* 2020; 26: 1207–1218.
77. Sood R, Yang Y, Taheri S, et al. Increased apparent diffusion coefficients on MRI linked with matrix metalloproteinases and edema in white matter after bilateral carotid artery occlusion in rats. *J Cereb Blood Flow Metab* 2009; 29: 308–316.
78. Kretz M, Eckardt D, Kruger O, et al. Normal embryonic development and cardiac morphogenesis in mice with Wnt1-Cre-mediated deletion of connexin43. *Genesis* 2006; 44: 269–276.
79. Talhouk RS, Zeinieh MP, Mikati MA, et al. Gap junctional intercellular communication in hypoxia-ischemia-induced neuronal injury. *Prog Neurobiol* 2008; 84: 57–76.